Hindawi
International Journal of Aerospace Engineering
Volume 2022, Article ID 6819836, 16 pages
https://doi.org/10.1155/2022/6819836

Research Article

Effects of Geometry of Plenum Chamber on Losses in the Bleed System of an Axial Compressor

Yuancheng Shi,[1] **Qingguo Kong**,[1] **and Wei Jia**[2]

[1]*Sino-European Institute of Aviation Engineering, Civil Aviation University of China, 2898 Jinbei Road, Tianjin, China*
[2]*Institute of Safety Science and Engineering, Civil Aviation University of China, 2898 Jinbei Road, Tianjin, China*

Correspondence should be addressed to Qingguo Kong; qgkong@cauc.edu.cn

Received 7 February 2022; Revised 29 June 2022; Accepted 16 July 2022; Published 2 August 2022

Academic Editor: Rosario Pecora

To study how the geometry of the plenum chamber in the bleed system of an axial compressor influences the losses therein and to establish a theoretical loss model for this system, a 1.5-stage axial compressor with a bleed system is studied numerically by means of computational fluid dynamics (CFD). The results show that losses in the bleed system occur mainly in the axisymmetric bleed slot and plenum chamber, accounting for ca. 85% of the total loss. For a bleed system with a vertical axisymmetric slot, the loss is more sensitive to the radial height than to the axial width of the plenum chamber. A loss model for each part of the bleed system is established via theoretical analysis, and then, a model of the overall bleed system is established by combining these submodels. The predictions of the theoretical loss model agree well with the CFD results: the maximum prediction error for the coefficient of the stagnation pressure loss in the bleed system is −1.38%, and the average prediction error is −0.8%. This loss model can be used when designing the geometry of a bleed system.

1. Introduction

In an aeroengine, depending on the operating conditions of the engine and the aircraft, the bleed system removes air flow with appropriate pressure and temperature through one or several compressor stages for cabin pressurization, wing thermal anti-icing, engine inlet anti-icing, and combustor and turbine cooling [1], all of which are necessary for normal engine operation and aircraft flight requirements. The bleed rate is between 1% and 5% of the mainstream flow during design operation and may increase during off-design operation. To satisfy the bleed air requirement of other systems and mitigate its impact on cycle efficiency, the loss mechanism of the bleed system on the mainstream flow and the losses within the bleed system must be investigated.

The bleed system consists of the bleed slot or a set of holes on the compressor casing, an annular plenum chamber, and the off-take ducts. The bleed shot or holes are used to extract air from the mainstream of the compressor, and a good design for the bleed slot configuration can reduce the secondary flow losses in the endwall region in certain conditions. Previous studies have investigated how the bleed slot shape—e.g., circular, rectangular, or axisymmetric—affects the mainstream flow [2, 3], and the results show that axisymmetric and circular slots are more effective in controlling the mainstream flow and generate lower bleeding losses. The bleed slot has different effects on the mainstream flow for different bleed positions in the blade passage and different bleed rates [4–6]. A proper bleed scheme can remove the low-energy fluid in the boundary layer and suppress the flow separation in the corner region of blade passage, thereby increasing both the adiabatic efficiency and the stall margin of the compressor [7–9].

Meanwhile, normal operation of the engine's secondary air system—which includes the bleed system—has an essential impact on the engine's behavior. Many scholars have modeled and analyzed the whole secondary air system, considering each of its elements as a "black box" and establishing the connections among them. The network of the secondary air system is drawn, and the conditions of each element during different phases are predicted using analysis codes (e.g., ESMS) [10–12]. However, unlike those simplified quasi-one-

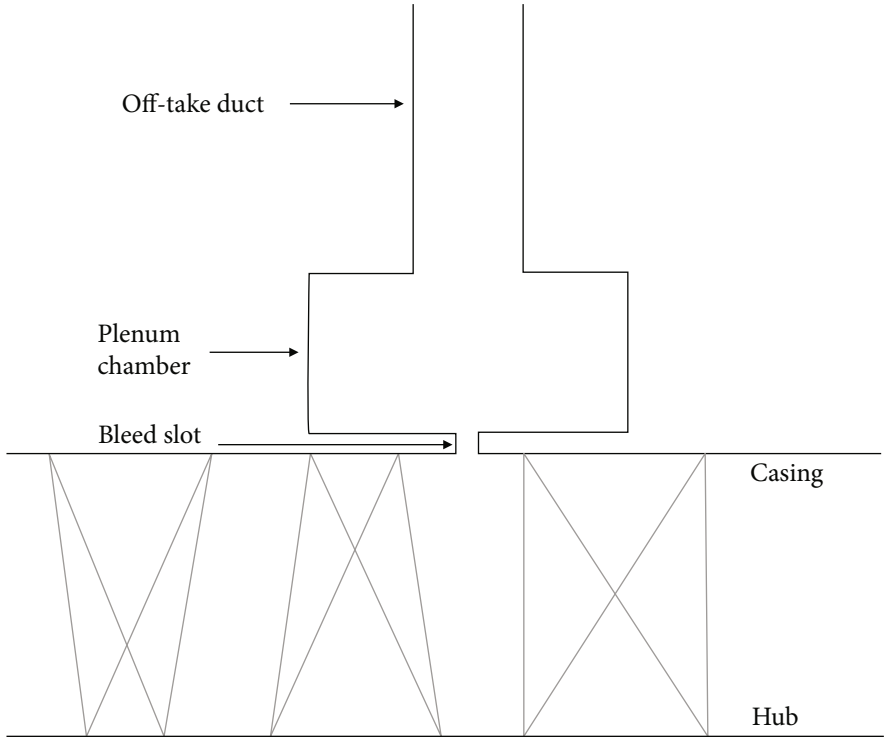

Figure 1: Meridional cross-section of compressor.

dimensional models, the flow within the compressor bleed system is strongly three-dimensional and the different parts interact with each other. To predict the performance of the bleed system accurately during the design process, it is necessary to obtain its internal flow characteristics and identify the loss mechanism.

Grimshaw et al. [13] studied the loss mechanism in the bleed system and concluded that there are two main sources of losses therein: (i) the shear stresses generated between the high-speed jet and the slot wall and (ii) the viscous mixing between the jet and the low-speed fluid in the plenum chamber. Gomes et al. [14] investigated how different off-take duct arrangements affect the flow in the bleed system, including double and quadruple distributions, and the choice of arrangement has a strong effect on the circumferential flow pattern in the plenum chamber. Peltier et al. [15] designed a new structure for the slot inlet—known as a "lip"—in which a circular arc with a certain radius is used at the inlet of the slot, instead of a right angle. This structure sacrifices the uniformity of the mainstream static pressure distribution to reduce the total pressure loss at the slot inlet.

In the bleed system, the most complicated flow phenomena are those in the plenum chamber. Gomes et al. [16] examined the loss generation mechanism in a bleed system whose plenum chamber had two different heights at different bleed rates; their results showed that the total pressure loss was between one and 1.5 dynamic heads when the bleed rate was increased from zero to 15%, and the loss within the plenum chamber increased with increasing plenum-chamber height. Schwarz [17] and Peltier et al. [18] studied the flow patterns inside the plenum chamber experimentally, finding that the flow therein is dominated by either a circumferential vortex or a pair of vortices with opposite rotational directions; the flow structure in the plenum chamber could be changed by varying the bleeding parameters.

Table 1: Geometric parameters of plenum chamber.

	IGV	Rotor	Stator
Hub-to-tip ratio	0.545	0.556	0.633
Height (mm)	88	86	71
Blade count	38	25	40
Rotation speed (rpm)	17000		
Tip clearance (mm)	0.03		
Width of bleed slot (L_x) (mm)	1.825		
Radial height of plenum chamber (mm)	10/20/44/60/76		
Axial width of plenum chamber (mm)	43/60/86/100/136		

However, the previous studies were all aimed at analyzing the flow patterns for a specific bleed structure, and there is yet to be a low-dimensional model that can predict the loss characteristics of the bleed system in the early design phase. The present paper investigates how different geometric parameters influence the internal flow of the plenum chamber and the loss of the bleed system. The effects of the radial height and axial width of the plenum chamber on the flow loss of the bleed system are evaluated separately. A loss model of each part of the bleed system is established via theoretical analysis, and then, a loss prediction model of the overall bleed system is established by combining these submodels.

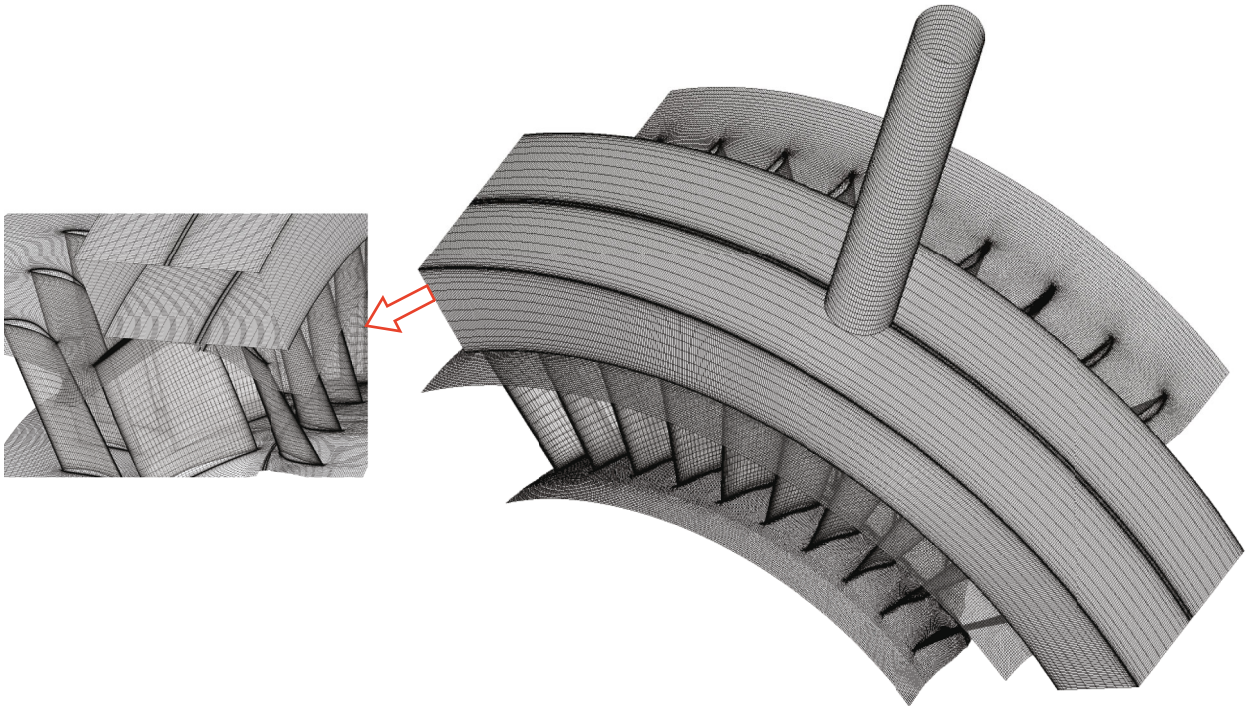

Figure 2: Structured mesh of compressor bleed system.

2. Geometries and Numerical Methods

Herein, a 1.5-stage low-speed subsonic compressor is studied, comprising an inlet guide vane (IGV), a rotor, and a stator, as shown in Figure 1. To study the compressor bleed system, an external bleed system connected to the casing was designed. In total, the bleed system is divided into three main parts: (i) the axisymmetric vertical slot, which is located between the rotor and the stator, (ii) the plenum chamber, and (iii) the off-take duct. To investigate the relationship between the loss of the bleed system and the geometric parameters of the plenum chamber as given in Table 1, the blade height H (71 mm) of the third row of stators was used as the length scale. The radial height was varied from $0.14H$ to $1.07H$, and the axial width was varied from $0.61H$ to $1.92H$, and how varying these two geometric parameters of the plenum chamber affected the loss of each part of the bleed system was evaluated.

Numerical simulations were performed using the commercial computational fluid dynamics (CFD) package Ansys CFX, which is a Reynolds-averaged Navier–Stokes code. The discretization schemes and solver parameters were the advanced scheme with high resolution, and the residual type was RMS with a high target that was 10 minus six. A periodic quarter-annulus sector was modeled to capture the circumferentially nonuniform flow in the plenum. For the mesh, a structured mesh, as shown in Figure 2, was generated using the commercial software Pointwise [19], and the total grid size was 10 128 431. The mesh had two parts: (i) the blade passage and (ii) the bleed system. The "HO" topology was used to generate the mesh: "O" blocks were used to grid the blade surfaces, rotor tip gap, and off-take duct, with "H" blocks used elsewhere. Figure 3 shows the four parts of computation domain in different colors, respectively, IGV, rotor, stator, and exit. The mesh height adjacent to the blade surface was set to 0.001 mm, thereby ensuring that the nondimensional wall cell size y^+ was ca. 1. Figure 4 shows the y^+ of the blade surface. The mixing-plane model was used to handle the stage interface.

Before conducting the study, the accuracy of the simulation results was assessed. Table 2 compares the CFD and experimental results for the mass flow rate and pressure ratio at the design point, and Figure 5 compares the CFD and experimental results for the compressor. As shown, the error between the CFD and experimental results at the design point is within 2%, which indicates that the former agree well with the latter.

Grid independence was checked for the bleed system, with four grids with 0.76 M, 1 M, 1.25 M, and 1.5 M finite volumes in the plenum chamber created and carefully studied. For the different numbers of grid points, Figure 6 shows the coefficient of the stagnation pressure loss (SPL) in the plenum chamber, and Figure 7 shows the exit average velocity. Thereafter, the 1.25 M grid was chosen for its ability to describe the flow in the plenum chamber accurately but with less computational burden. Table 3 gives the numbers of grid points used for the different parts of the bleed system.

3. Results and Discussion

3.1. Flow Structure in Bleed System. Bleeding air from the main flow impacts the flow characteristics in a small region near the shroud, as shown in Figure 8. The flow characteristics in each part of the bleed system differ significantly, and as shown in Figure 9 for a medium bleed rate, the flow is separated into two zones in the bleed slot. The recirculation

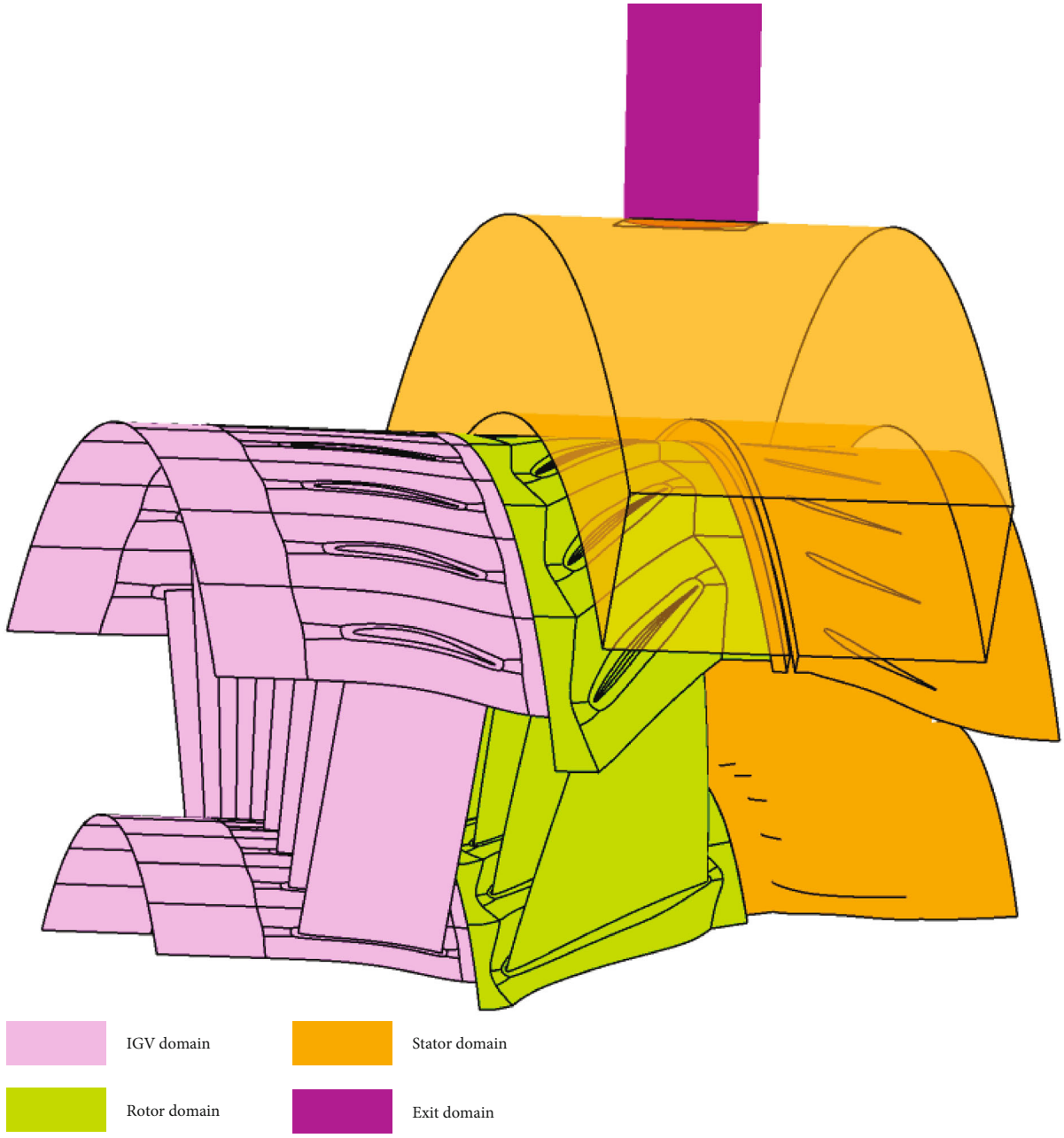

Figure 3: Computational domain.

zone—which occupies approximately half of the axial width of the slot—is generated by a portion of the low-speed flow separated from the plenum chamber; this zone contains a separation bubble that blocks the flow through the slot. The other zone is the high-speed jet flowing into the plenum chamber along the slot wall. The bleed rate has a significant impact on the flow in the slot, and Figure 10 shows the flow characteristics in the slot with low and high bleed rate. The separation bubble shrinks steadily with increasing bleed rate, and the jet accelerates, thereby changing its direction slightly at the slot exit.

The bleed flow undergoes a sudden expansion as it leaves the slot, and the jet dynamic head is dissipated by the mixing with the low-speed fluid in the plenum chamber; the bleed flow then rolls into two circumferential vortices with opposite rotations. The off-take duct is responsible for the inhomogeneity of the circumferential flow in the bleed system; nevertheless, the off-take duct has only a minor influence on the slot, affecting mostly the flow in the plenum chamber. The circulation of radial flow is great near the off-take duct (see Figure 11(a)), and at the contact between the off-take duct and the plenum chamber, the radial velocity varies slightly. Away from the off-take duct, the radial velocity drops to zero (see Figure 11(b)) because of the effect of the upper wall of the plenum chamber, and the fluid develops along the axial direction.

With relatively small radial height, the plenum chamber contains a pair of vortices with comparable sizes but opposite rotations, as shown in Figures 12(a) and 12(b). With

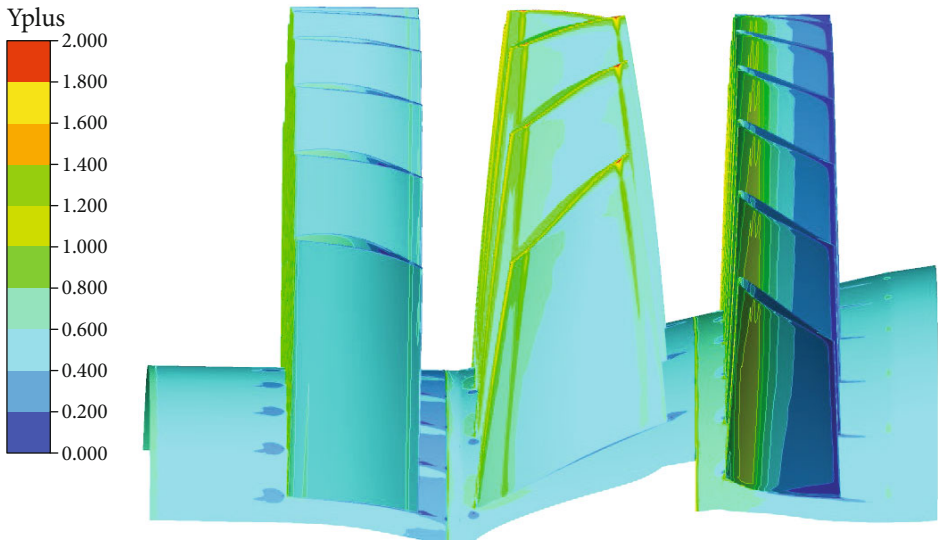

Figure 4: y^+ of the blade surface.

Table 2: Comparison of numerical simulation and experimental results.

	Experiment [20]	CFD
Pressure ratio	1.30	1.3069
Corrected mass flow rate (kg/s)	13.4	13.406

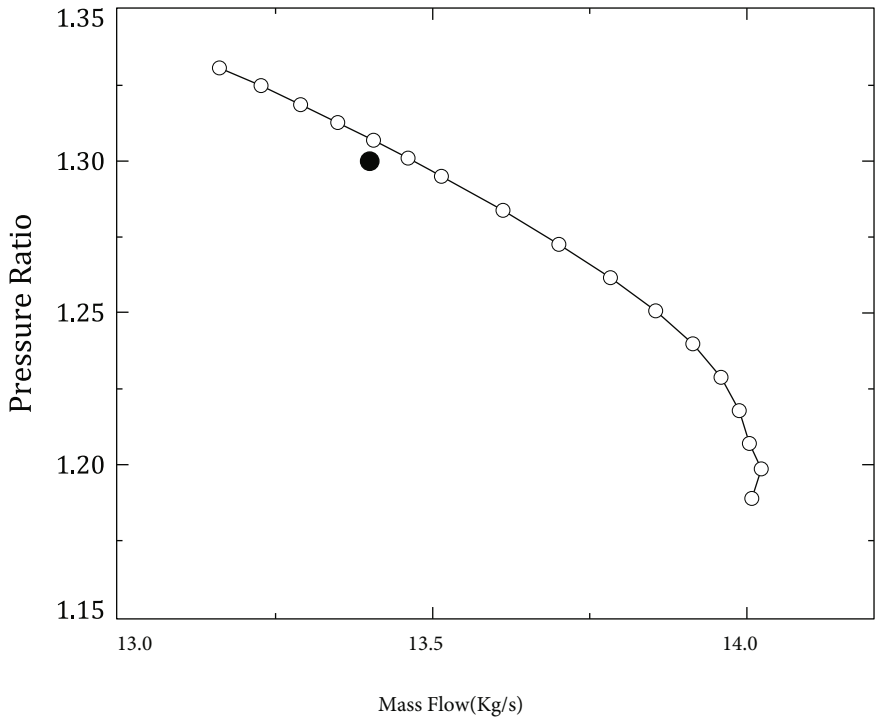

Figure 5: Compressor map.

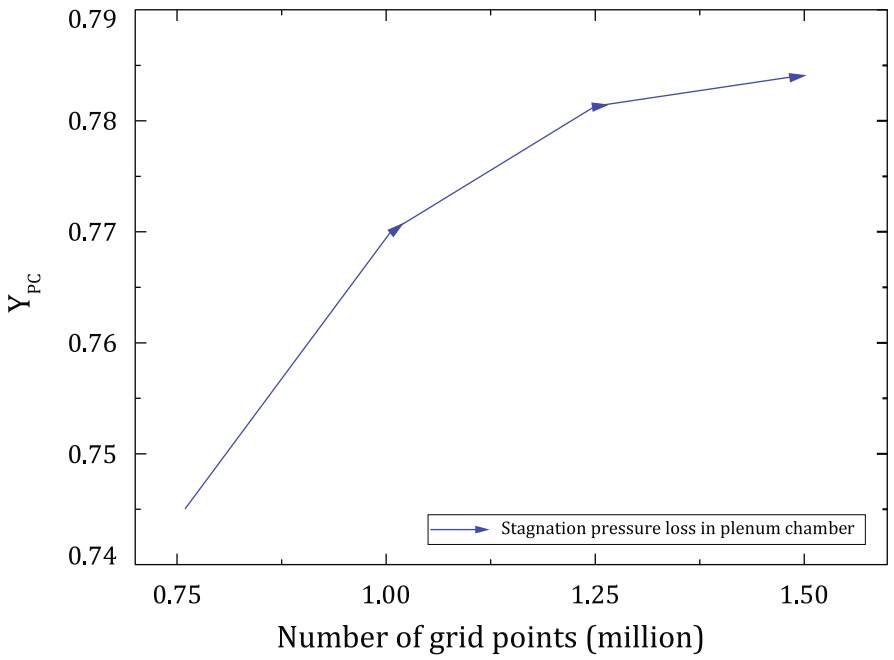

Figure 6: Coefficient of stagnation pressure loss (SPL) in plenum chamber for different numbers of grid points.

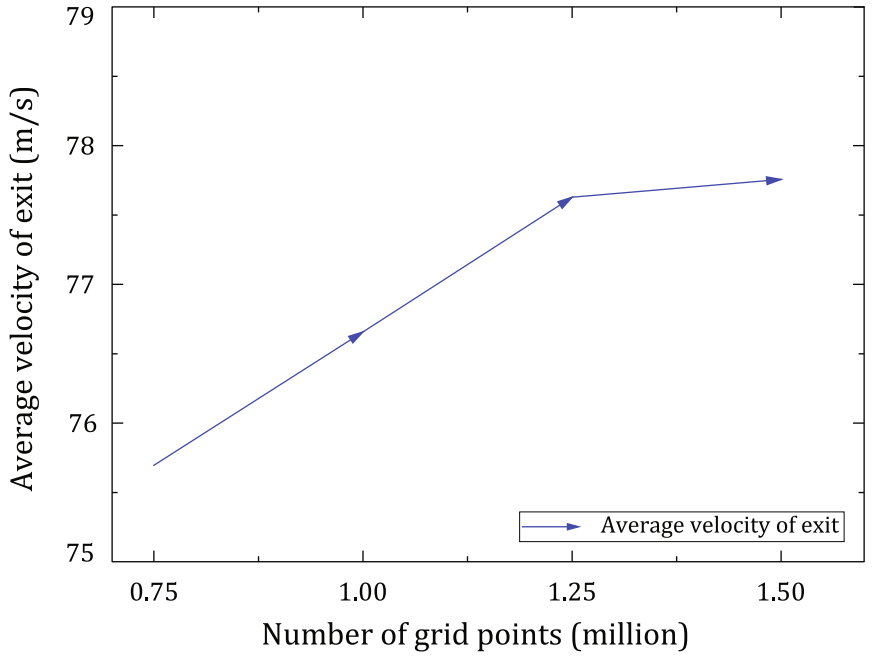

Figure 7: Average exit velocity for different numbers of grid points.

Table 3: Numbers of grid points used for bleed system.

	Bleed slot	Plenum chamber	Off-take duct
Number of points (axial × radial × circumferential)	13 × 29 × 441	70 × 41 × 441	667 578 (total)

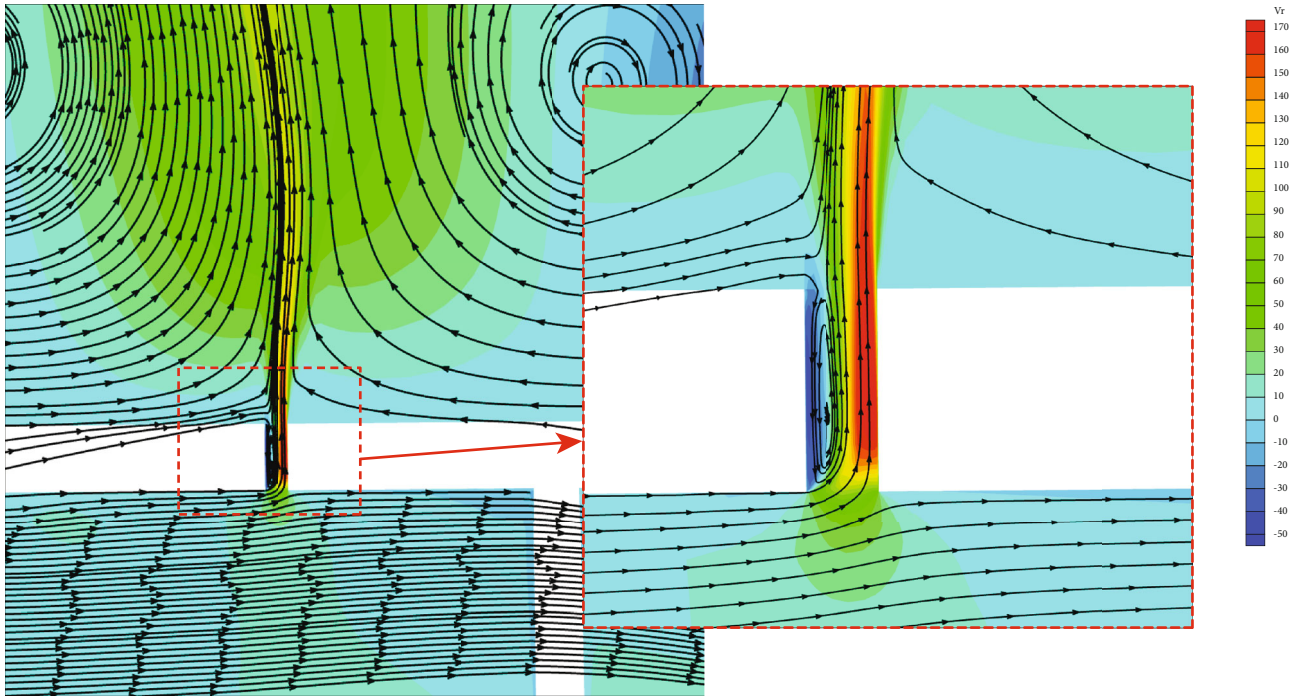

Figure 8: Flow characteristics near the shroud.

increasing radial height of the plenum chamber, the vortices grow and develop different sizes, as shown in Figures 12(c) and 12(d). The intake of the off-take duct has a zone of high radial velocity that reduces progressively with increasing radial height, indicating the uniformity of the inlet flow of the off-take duct. However, the radial height has only a minor impact on the flow in the slot.

The distributions of velocity and streamlines are used to analyze the flow characteristics inside the bleed system, and quantitative analytical methods are used to investigate the losses in the various components of the bleed system to identify its loss mechanism.

3.2. Coefficient of Stagnation Pressure Loss. The bleed system loss depends on both the compressor operating point and the bleed rate, therefore requiring a metric that removes this dependence [20]. The SPL coefficient for the flow passing through the bleed system is defined as

$$Y_p = \frac{P_{0\mathrm{CVin}} - P_{0e}}{(P_0 - P)_{\mathrm{CVin}}}, \tag{1}$$

where the subscript CVin refers to the inlet of the control volume (bleed slot inlet) and the subscript e refers to the exit of the control volume (off-take duct outlet).

The SPL coefficients for the slot, plenum chamber, and off-take duct are calculated separately to analyze the loss distribution in the bleed system, of which the plenum-chamber SPL accounts for 60% of the total loss. Figure 13 shows how each part of the loss changes with increasing radial height, and the percentage of the plenum-chamber loss is still increasing. With a certain bleed rate, which is ca. 20% of the total loss, the SPL in the slot is kept at a constant level, whereas the SPL in the off-take duct is decreasing gradually. The total loss of the bleed system decreases and then tends to stabilize. Figure 14 shows how the loss in each part changes with increasing axial width: the loss in the slot changes by only a little, whereas the loss in the plenum chamber increases gradually. The additional loss is due mainly to the friction at the plenum-chamber wall, but this causes the uniformity of the off-take duct inlet to tend to unity and reduces the partial loss in the off-take duct.

The main losses in the bleed system are determined by calculating the SPL coefficient of each component. Identifying the loss mechanism requires investigating the specific regions of loss generation, the intensities of multiple losses, and how they are influenced by the radial height and axial width.

3.3. Entropy Generation. In fluid flow, irreversibility arises because of heat transfer and viscosity. The entropy generation rate can be expressed as the sum of the contributions of the viscous and thermal effects, so it depends functionally on the local values of velocity and temperature in the domain of interest. In the bleed system, both the temperature and velocity fields are known, and the local volume entropy generation rate can be calculated as [21]

$$\dot{S}_{\mathrm{gen}} = \left(\dot{S}_{\mathrm{gen}}\right)_{\mathrm{fric}} + \left(\dot{S}_{\mathrm{gen}}\right)_{\mathrm{heat}}, \tag{2}$$

where $\left(\dot{S}_{\mathrm{gen}}\right)_{\mathrm{fric}}$ and $\left(\dot{S}_{\mathrm{gen}}\right)_{\mathrm{heat}}$ represent the entropy generation due to viscous and thermal effects, respectively, and are defined as

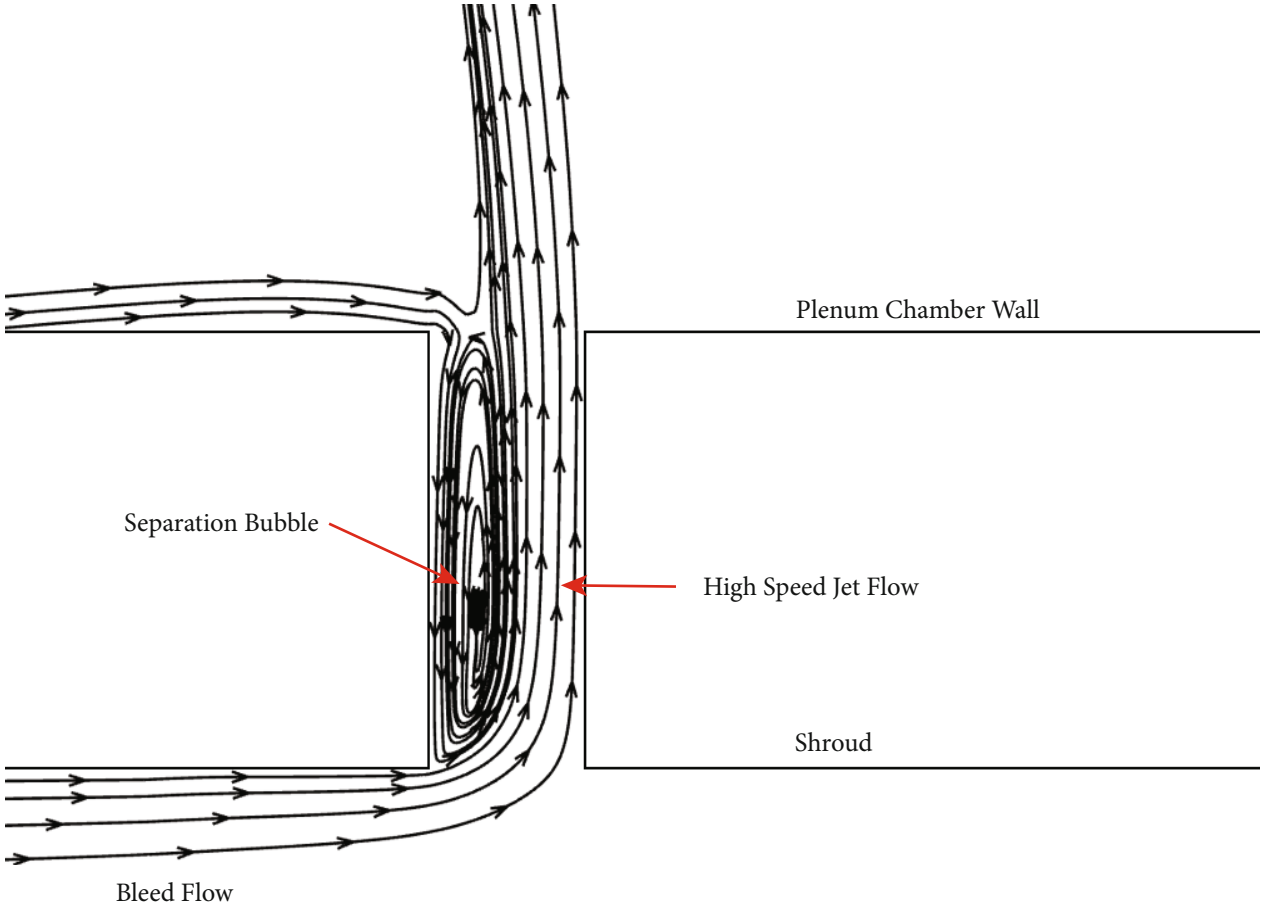

Figure 9: Flow diagram in slot with medium bleed rate.

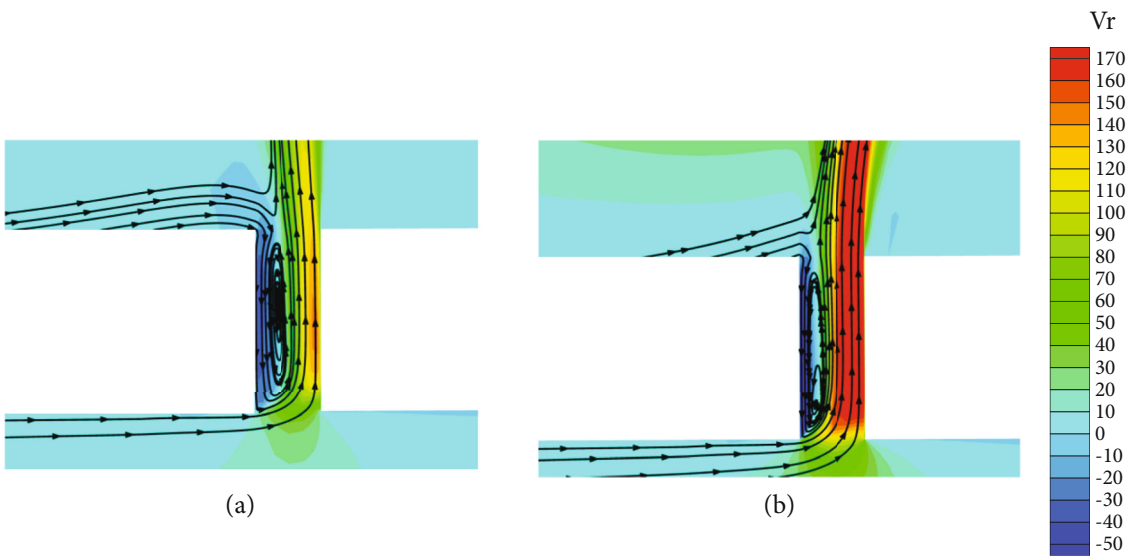

Figure 10: Flow in slot with (a) low and (b) high bleed rate.

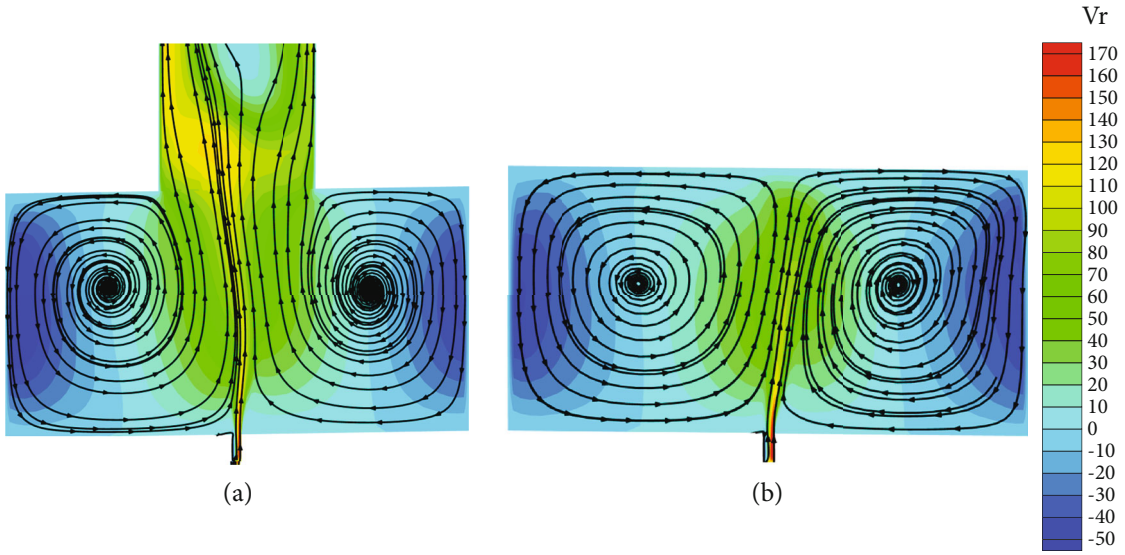

Figure 11: Distributions of radial velocity and streamlines in meridional plane at two different positions with $D_r/H = 0.62$: (a) plane at center of off-take duct and (b) plane 15° from off-take duct.

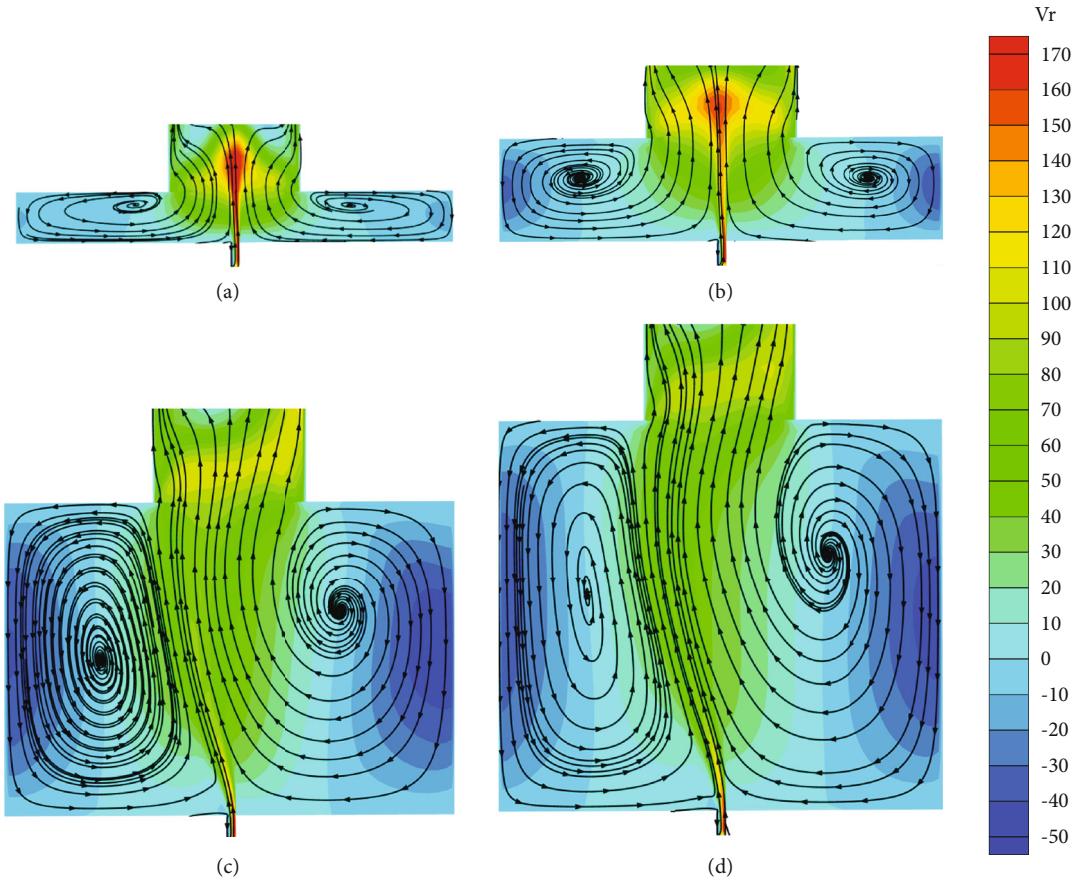

Figure 12: Distributions of radial velocity and streamlines in meridional plane with differing radial height: $D_r/H =$ (a) 0.14, (b) 0.28, (c) 0.85, and (d) 1.07.

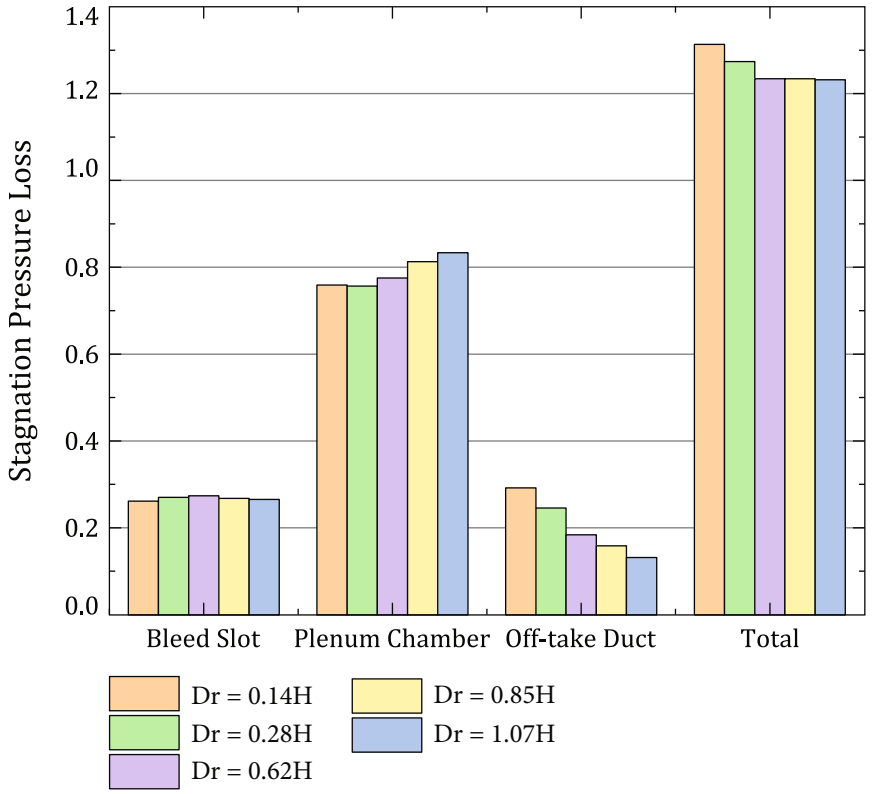

Figure 13: SPL coefficient of each part of bleed system with differing radial height.

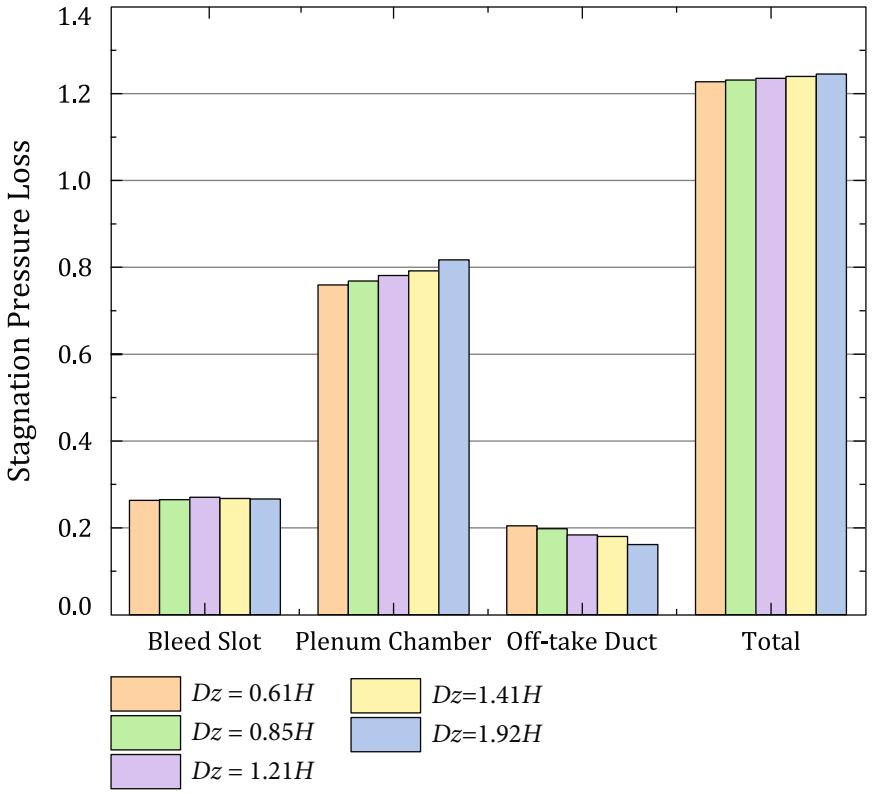

Figure 14: SPL coefficient for each part with differing axial width.

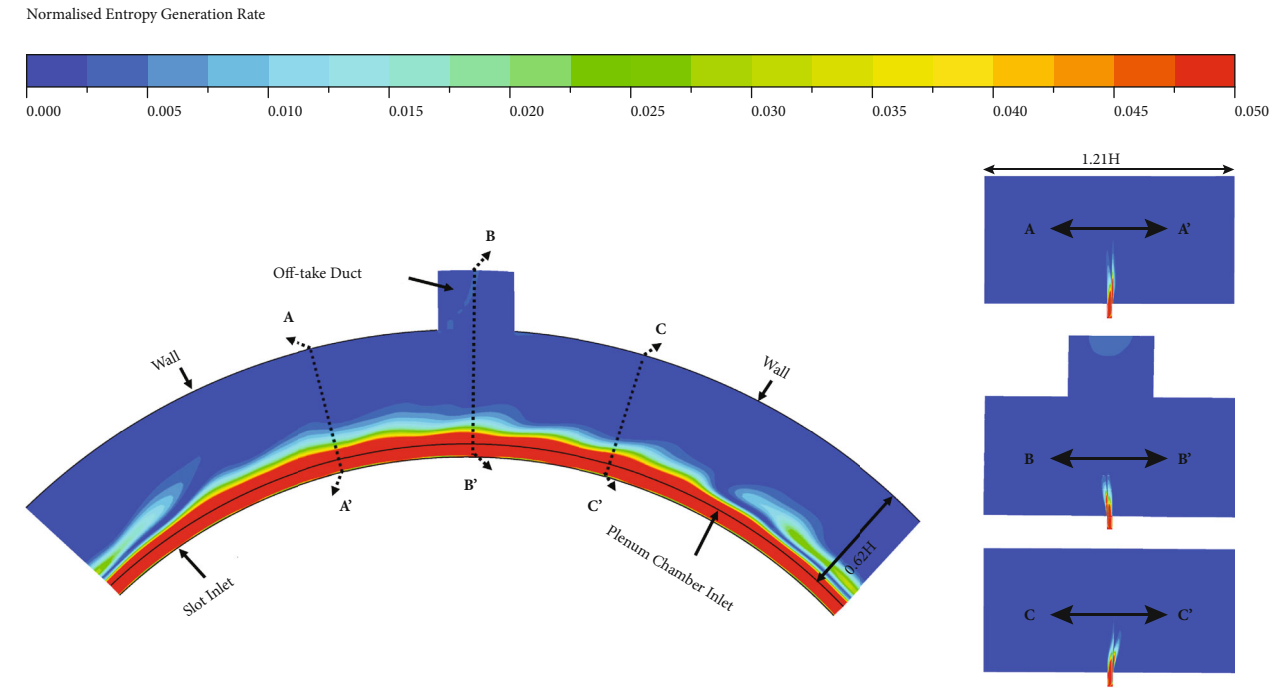

Figure 15: Normalized entropy generation rate of bleed system for plenum chamber with a radial height of 0.62H and an axial width of 1.21H.

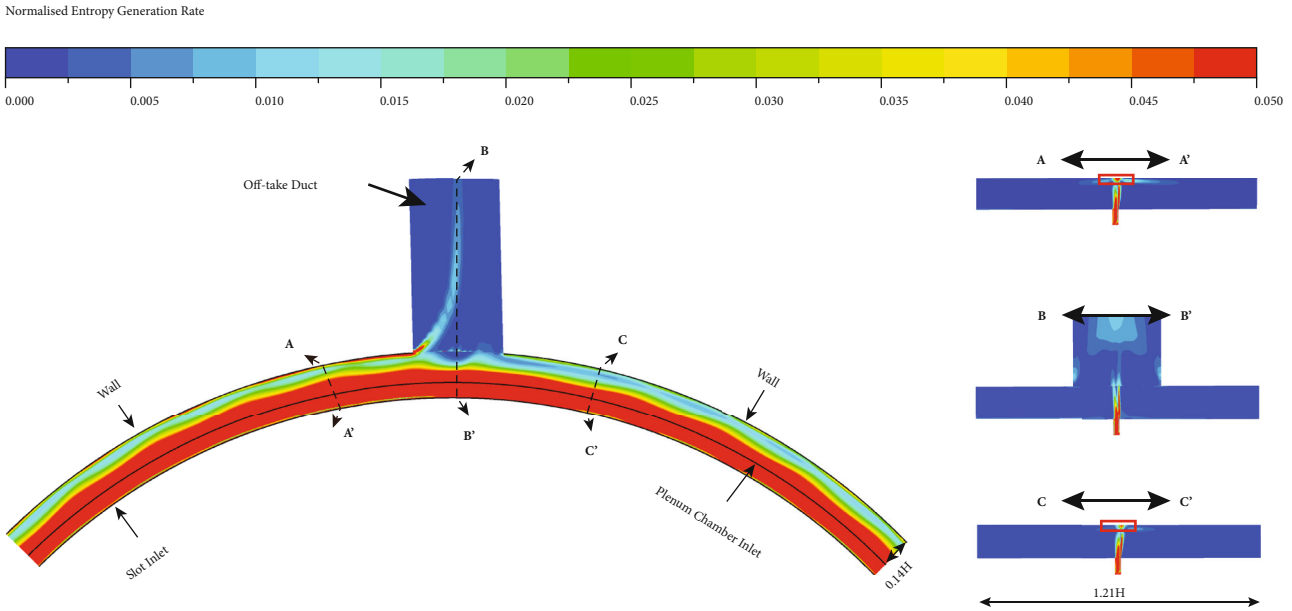

Figure 16: Normalized entropy generation rate of bleed system for plenum chamber with a radial height of 0.14H and an axial width of 1.21H.

$$\left(\dot{S}_{\text{gen}}\right)_{\text{fric}} = \frac{1}{T}\tau_{ij}\frac{\partial V_i}{\partial x_j},$$
$$\left(\dot{S}_{\text{gen}}\right)_{\text{heat}} = \frac{k}{T^2}\left(\frac{\partial T}{\partial x_j}\right)^2, \quad (3)$$

where τ_{ij} is the viscous shear stress and k is the thermal conductivity.

Flow regions in which losses occur can be identified directly by evaluating the local volumetric entropy generation rate. To unify the evaluation criteria, the volumetric entropy generation rate of the bleed system is normalized as

$$\tilde{\dot{S}}_{\text{gen}} = \frac{T_{\text{CVin}}\,\dot{S}_{\text{gen}}}{\rho V_{\text{CVin}}^3/L_x}, \quad (4)$$

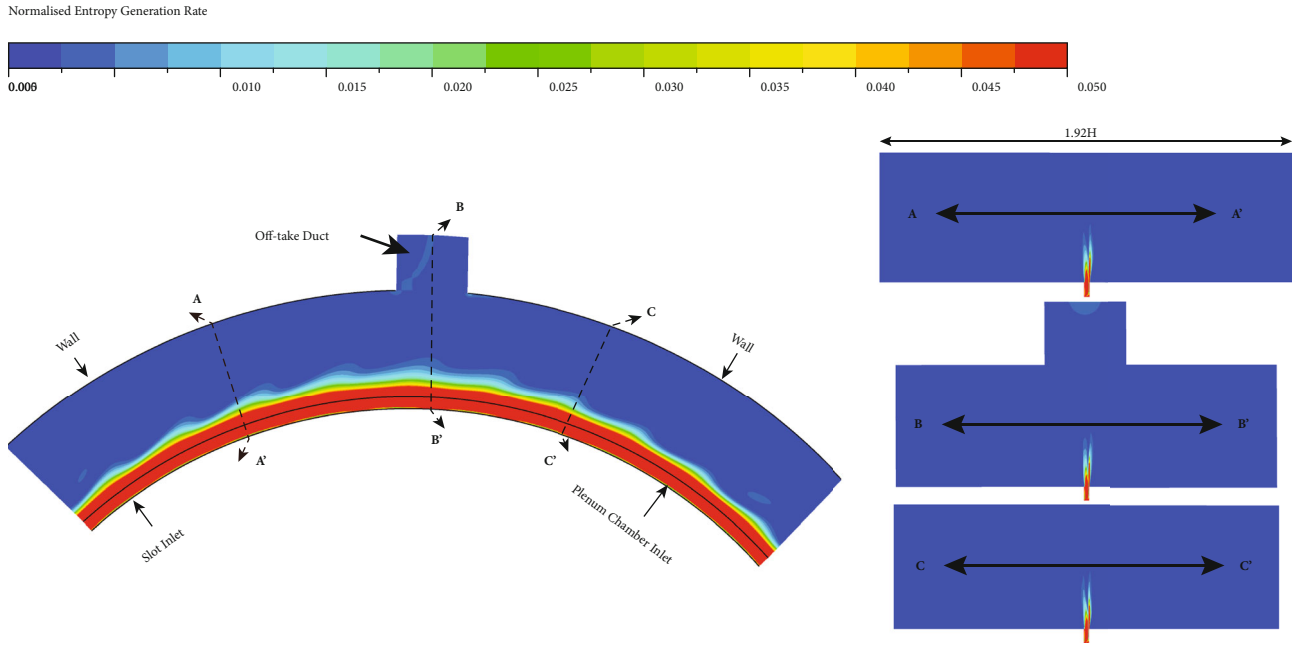

Figure 17: Normalized entropy generation rate of bleed system for plenum chamber with a radial height of $0.62H$ and an axial width of $1.92H$.

where $T_{\mathrm{CVin}} = P_{\mathrm{CVin}}/\rho R$ and $V_{\mathrm{CVin}} = \sqrt{2(P_0 - P)_{\mathrm{CVin}}/\rho}$ are the temperature and speed, respectively, at the inlet of the bleed system, and L_x is the axial width of the slot inlet.

To describe the complex three-dimensional flow in the bleed system, the volumetric entropy generation rate in the bleed system is described by the iso-Z surface and the iso-θ cross-section; in the corresponding figures, the former is shown on the left and the latter is shown on the right side, where B-B$'$ is the central cross-section of the off-take duct and A-A$'$ and C-C$'$ are those $\pm 15^\circ$ from the center of the off-take duct, respectively. According to the iso-Z cross-section, the entropy generation rate is high in the slot and plenum chamber, and Figures 15 and 16 show the normalized entropy generation rate for two different values of the plenum-chamber radial height. The high-speed jet from the slot is not decelerated adequately by the limited radial height, and its influence continues into the off-take duct, resulting in greater loss therein. At the section far from the off-take duct, the high-speed jet impacts the upper wall of the plenum chamber, forming an impact zone (red region in Figure 16), and the jet therein decelerates rapidly and develops laterally. Because of viscosity, the lateral development of the jet thickens the boundary layer and increases the friction loss; however, compared with the mixing loss generated by the jet and the loss in the impact zone, this part of the loss can be ignored. The high-speed jet from the slot is decelerated more with increasing radial height; the speed at which it impacts the upper wall of the plenum chamber decreases, as does the loss in the impact zone. Figures 15 and 17 show the normalized entropy generation rate for two different values of the plenum-chamber axial width. Comparing the iso-Z cross-sections shows that the larger the axial width, the smaller the circumferential inhomogeneity caused by the off-take duct, but the flow characteristics of the bleed system are not affected significantly, which means that the axial width has little effect on the loss in the bleed system.

4. Theoretical Model

The influences of different values of the radial height and axial width of the plenum chamber on the loss in the bleed system were studied, and it was found that in the bleed system with a vertical slot, the axial width has little effect, whereas the radial height has a greater effect. Herein, theoretical submodels of each component of the bleed system are established based on the influence of the radial height of the plenum chamber.

4.1. Off-Take Duct Loss Model. If the inlet condition of a pipe is uniform incoming flow, then previous research shows that the flow SPL in the pipe can be calculated as [22]

$$\Delta P_{0(c-e)} = \lambda \rho \frac{l}{d} \frac{V^2}{2}, \tag{5}$$

where λ is the friction factor of the pipe and depends on its diameter, l is the length of the pipe, d is the diameter of the pipe, and V is the flow speed at the pipe inlet. However, in the bleed system, the inlet condition of the off-take duct is often nonuniform, and so the above flow SPL equation is no longer applicable. Instead, we define here the inlet uniformity, which is used to calculate the off-take duct flow SPL, i.e., [23]

$$N = \frac{1}{\dot{m}} \int \left(V/\bar{V}\right)^3 d\dot{m}, \tag{6}$$

where $\bar{V}$ is the average flow speed at the inlet. Correcting the velocity with the inlet uniformity, the submodel of the off-

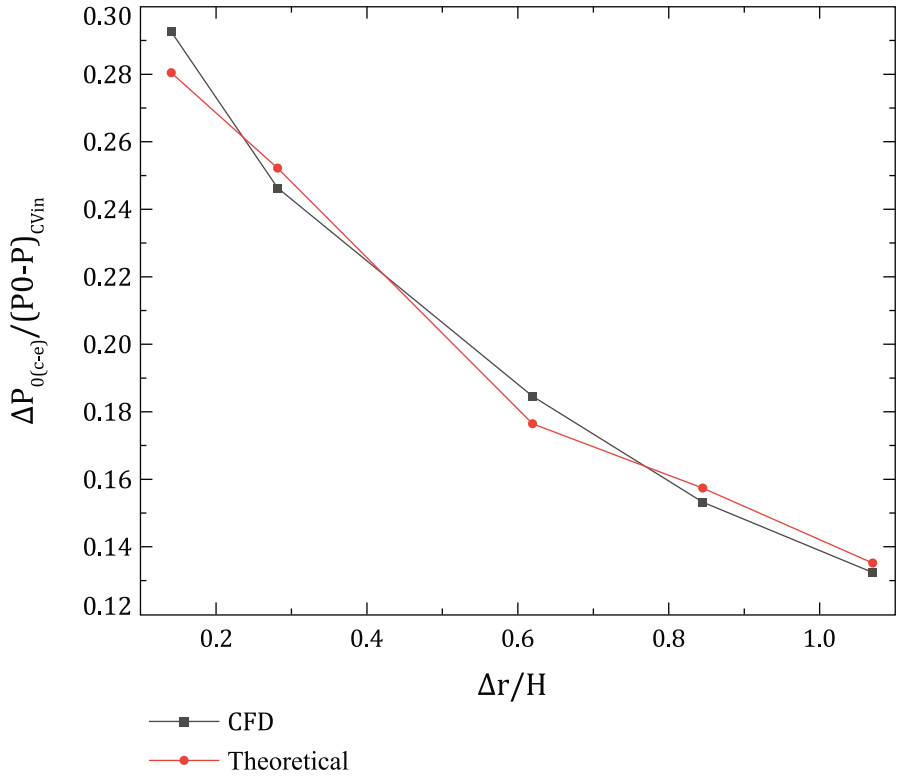

Figure 18: Comparison of results of theoretical model and CFD for SPL coefficient in off-take duct with differing radial height of plenum chamber.

take duct is obtained as

$$\Delta P_{0(c-e)} = \lambda\rho\frac{l}{d}\frac{(NV)^2}{2} = \lambda\rho N^2\frac{l}{d}\frac{V^2}{2}. \quad (7)$$

Figure 18 compares the theoretical and CFD results for the SPL coefficient in the off-take duct with differing radial height of the plenum chamber; they agree well, with a maximum error of −4% and an average error of 1%. The loss coefficient in the off-take duct decreases with increasing radial height of the plenum chamber, the main reason being that the uniformity of the off-take duct inlet decreases with increasing radial height. The corrected equation shows that the uniformity has a significant influence on the loss in the off-take duct.

4.2. Slot Loss Model. The loss mechanism in both the slot and the off-take duct is the viscous shear force, so it is reasonable to use the same SPL model for both. However, because the slot is rectangular, the diameter is replaced by the hydraulic diameter, which is defined as

$$D = \frac{4A}{C}, \quad (8)$$

where A is the area of the rectangular section and C is its perimeter. The submodel of the slot is obtained by replacing d in the corrected equation by D, i.e.,

$$\Delta P_{0(\mathrm{CVin}-s)} = \lambda\rho N^2\frac{l}{D}\frac{V^2}{2}. \quad (9)$$

Table 4: Comparison of results of theoretical model and CFD for average SPL coefficient in slot.

	Model	CFD	Error
$\Delta P_{0(\mathrm{CVin}-s)}/(P_0 - P)_{\mathrm{CVin}}$ in slot	0.2402	0.2561	−6.2%

The geometrical parameters of the plenum chamber have small influence on the SPL coefficient in the slot, so it is reasonable and convenient to investigate the average SPL coefficient of different cases. Table 4 compares the theoretical and CFD results for the average SPL coefficient in the slot; they agree well, but the theoretical model does not predict the loss due to the recirculation region in the slot, which leads to a smaller predicted value and is the main reason for the error.

4.3. Plenum-Chamber Loss Model. The loss mechanism in the plenum chamber is the viscous mixing between the high-speed jet from the slot and the low-speed fluid in the plenum chamber. This is similar to a free jet, for which there is no pressure gradient along the jet and the SPL is due to loss of kinetic energy. From previous work, the rate of decay of the energy of a free jet is described empirically as [24]

$$\Delta P_{0(s-c)} = \Delta E_k = (P_0 - P)_s\left(1 - \frac{2.853}{\sqrt{x/b_0}}\right), \quad (10)$$

where x is the distance along the jet and b_0 is the half-width at the beginning of the jet.

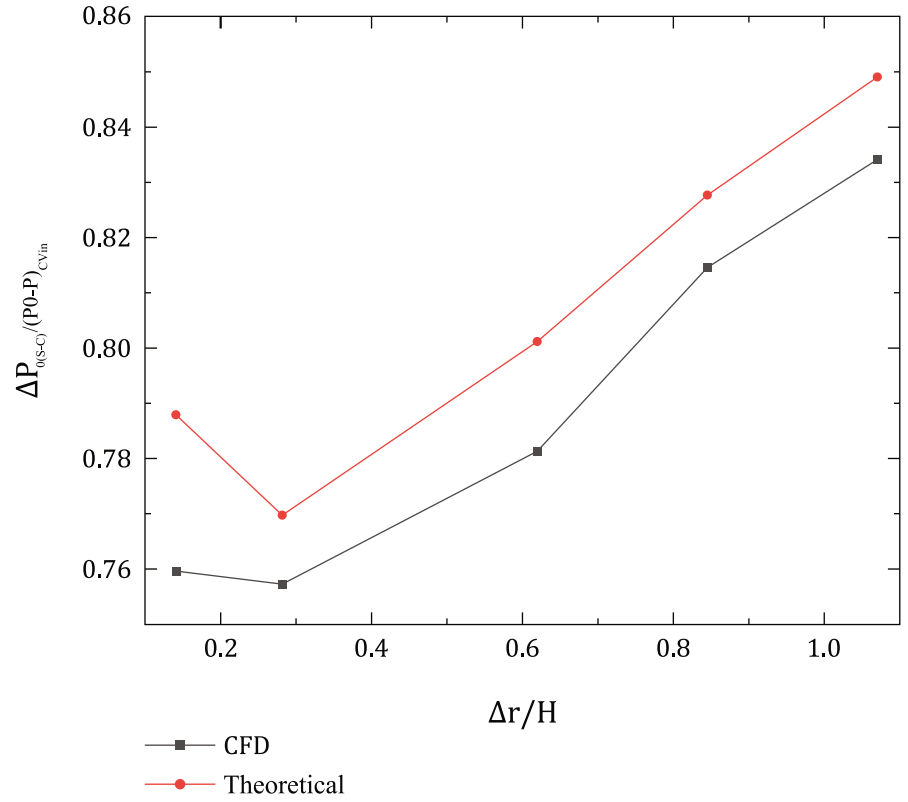

Figure 19: Comparison of results of theoretical model and CFD for SPL coefficient in plenum chamber with differing radial height of plenum chamber.

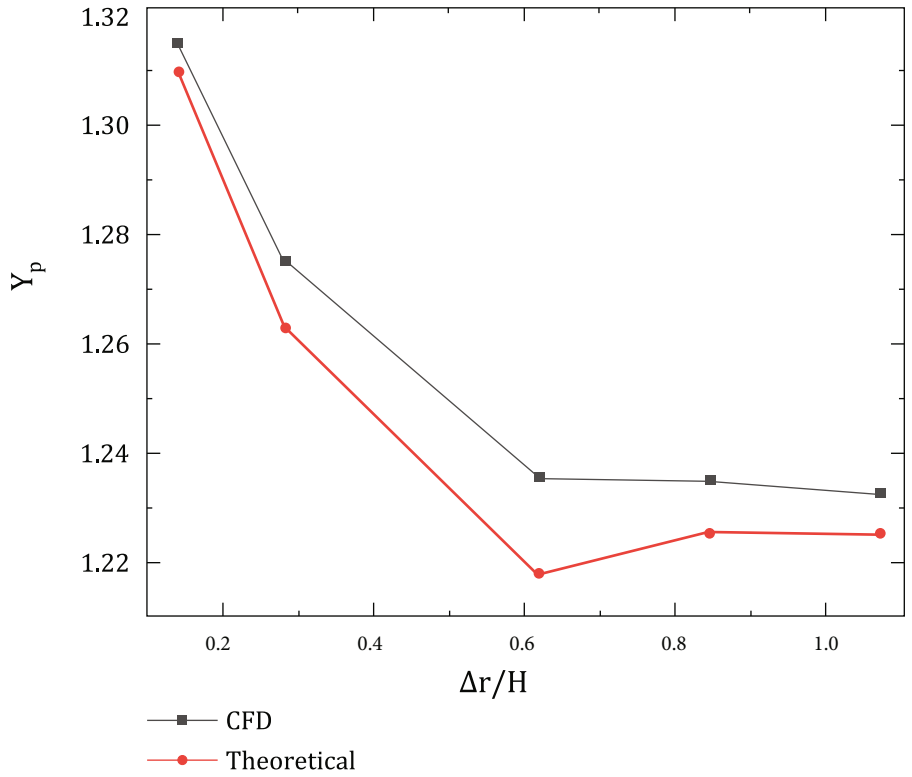

Figure 20: Comparison of results of theoretical model and CFD for SPL coefficient in bleed system with differing radial height of plenum chamber.

When the radial height of the plenum chamber is large, we can ignore the influence of its upper wall and consider the flow as a simple free jet. However, when the radial height is small, the influence of the upper wall on the jet cannot be ignored: the free jet becomes an impinging jet and the jet speed drops abruptly at the impact region, generating a reverse pressure gradient and hence an SPL. However, the literature appears to be lacking an empirical equation for the SPL of the impinging jet. Herein, to predict the SPL in the plenum chamber, we correct the kinetic energy decay rate of the free jet as

$$\widetilde{\Delta P_{0(s-c)}} = (P_0 - P)_s \left(\left(\frac{2.853}{\sqrt{x/b_0}} \right)^2 - \left(\frac{2.853}{\sqrt{x/b_0}} \right) + 1 \right). \quad (11)$$

The SPL coefficient in the plenum chamber with differing radial height is calculated using the corrected equation and compared with the CFD results, as shown in Figure 19. The two sets of results agree well, with a maximum error of 3.612% and an average error of 2.55%. The SPL coefficient in the plenum chamber decreases initially with increasing radial height and then increases: when the radial height of the plenum chamber is small, the SPL coefficient decreases with increasing radial height because the loss in the impact region decreases more than does the kinetic energy of the jet; when the radial height of the plenum chamber is large, the SPL coefficient increases with increasing radial height mainly because of the loss of jet kinetic energy. The presence of the offtake duct changes part of the jet flow in the plenum chamber, which is not predicted by the theoretical model.

4.4. Stagnation Pressure Loss in Bleed System. The loss in each part is normalized by the dynamic head of the bleed system inlet, the inlet conditions of each part are the outlet conditions of the previous part, and the total loss in the bleed system is the sum of the losses in its three constituent parts. Figure 20 compares the theoretical and CFD results for the SPL coefficient of the bleed system with differing radial height of the plenum chamber; they agree well, with a maximum error of −1.38% and an average error of −0.82%, indicating that the theoretical model can predict accurately the SPL coefficient in the bleed system.

The CFD and theoretical results show that narrowing the impact region in the plenum chamber requires choosing a proper radial height for the plenum chamber, which herein is greater than 0.6H. This minimizes the loss in the bleed system, which is useful for its geometrical design.

5. Conclusions

Herein, the flow characteristics and loss mechanism of the bleed system of an axial compressor were investigated, the bleed system was subjected to a comparative analysis for differing radial height and axial width of its plenum chamber, and a theoretical loss model was established. The following conclusions are drawn.

The main sources of loss in the bleed system are (i) the shear at the wall of the slot and (ii) the viscous mixing of the high-speed jet with the low-speed fluid in the plenum chamber, which together account for more than 85% of the total loss in the bleed system.

For the bleed system with differing radial height of its plenum chamber, the SPL coefficient decreases initially with increasing radial height and then tends to stabilize; by contrast, the axial width of the plenum chamber has no apparent effect on the SPL coefficient of the bleed system. This indicates that when the slot is vertical, the loss in the bleed system is sensitive to the radial height of the plenum chamber but not to its axial width.

When the radial height of the plenum chamber is small, the SPL coefficient decreases with increasing radial height because the loss in the impact region decreases more than does the jet kinetic energy, whereas when the radial height of the plenum chamber is large, the SPL coefficient increases with increasing radial height mainly because of the loss of jet kinetic energy.

A model was established that can predict the loss in the bleed system. Its results agreed well with those from CFD, with a maximum error of −1.38% and an average error of −0.82%, so the present loss model for the bleed system can be used to assist in the design progress.

Notations

A: Area (m^2)
b_0: Half-width of jet flow (mm)
C: Perimeter (m)
D: Hydraulic diameter (m)
d: Diameter (m)
H: Height of blade (mm)
k: Thermal conductivity (J/K/m/s)
l: Length (m)
L_x: Axial width of bleed slot inlet (mm)
N: Uniformity
P_0: Stagnation pressure (Pa)
P: Static pressure (Pa)
$\dot{S}_{gen}$: Volumetric entropy generation rate ($J/K/m^3/s$)
T: Temperature (K)
x: Jet flow distance (mm)
Y_P: Coefficient of stagnation pressure loss in bleed system
Y_{Pc}: Coefficient of stagnation pressure loss in plenum chamber
ρ: Density (kg/m^3)
τ_{ij}: Viscous shear stress (N/m^2)
λ: Friction factor of pipe
Dr: Radial height of the plenum chamber (m)
Dz: Axial width of the plenum chamber (m).

Subscripts

CVin: Inlet of bleed system
S: Slot outlet
c: Chamber outlet
e: Exit of bleed system.

Data Availability

Some or all data, models, or code that support the findings of this study are available from the corresponding author upon reasonable request.

Conflicts of Interest

The authors declare that they have no conflicts of interest.

Acknowledgments

The authors gratefully acknowledge the support of the Fundamental Research Funds for the Civil Aviation University of China (grant number 3122019182).

References

[1] D. G. Bogard and K. A. Thole, "Gas turbine film cooling," *Journal of Propulsion and Power*, vol. 22, no. 2, pp. 249–270, 2006.

[2] F. Conan, S. Savarese, and S. Moteurs, "Bleed airflow CFD modeling in aerodynamics simulations of jet engine compressors," *Turbo Expo: Power for Land, Sea, and Air*, vol. 78507, 2001.

[3] B. A. Leishman and N. A. Cumpsty, "Mechanism of the interaction of a ramped bleed slot with the primary flow," *Turbo Expo: Power for Land, Sea, and Air*, vol. 47306, pp. 187–198, 2005.

[4] B. A. Leishman, N. A. Cumpsty, and J. D. Denton, "Effects of bleed rate and end wall location on the aerodynamic behavior of a circular hole bleed off-take," *Journal of Turbomachinery*, vol. 129, no. 4, pp. 645–658, 2007.

[5] B. A. Leishman, N. A. Cumpsty, and J. D. Denton, "Effects of inlet ramp surfaces on the aerodynamic behavior of bleed hole and bleed slot off-take configurations," *Journal of Turbomachinery*, vol. 129, no. 4, pp. 659–668, 2007.

[6] S. R. Wellborn and M. L. Koiro, "Bleed flow interactions with an axial-flow compressor powerstream," in *38th AIAA/ASME/SAE/ASEE Joint Propulsion Conference & Exhibit*, Indianapolis, Indiana, 2002.

[7] B. Liu, X. Zhuang, G. An, and X. Yu, "Numerical and experimental study of bleed impact in multistage axial compressors," *Chinese Journal of Aeronautics*, 2022.

[8] E. M. V. Siggeirsson, N. Andersson, and M. Burak Olander, "Numerical and experimental aerodynamic investigation of an S-shaped intermediate compressor duct with bleed," *Journal of Turbomachinery*, vol. 143, no. 10, article 101003, 2021.

[9] K. Salmanov and H. Harb, "Data analysis for the aero derivative engines bleed system failure identification and prediction," *International Journal of Intelligent Systems and Applications*, vol. 13, no. 6, pp. 13–24, 2021.

[10] A. Foley, "On the performance of gas turbine secondary air systems," *Turbo Expo: Power for Land, Sea, and Air*, vol. 78521, 2001.

[11] K. J. Kutz and T. M. Speer, "Simulation of the secondary air system of aero engines," *Journal of Turbomachinery*, vol. 116, no. 2, pp. 306–315, 1994.

[12] C. Carcasci, B. Facchini, S. Gori, L. Bozzi, and S. Traverso, "Heavy duty gas turbine simulation: global performances estimation and secondary air system modifications," *Turbo Expo: Power for Land, Sea, and Air*, vol. 42398, pp. 527–536, 2006.

[13] S. D. Grimshaw, J. Brind, G. Pullan, and R. Seki, "Loss in axial compressor bleed systems," *Journal of Turbomachinery*, vol. 142, no. 9, 2020.

[14] R. A. Gomes, C. Schwarz, and M. Pfitzner, "Experimental investigation of a generic compressor bleed system," *Turbo Expo: Power for Land, Sea, and Air*, vol. 4241, pp. 241–249, 2006.

[15] V. Peltier, K. Dullenkopf, and H. J. Bauer, "Numerical investigation of the aerodynamic behaviour of a compressor bleed-air system," *Turbo Expo: Power for Land, Sea, and Air*, vol. 45608, 2014.

[16] R. Gomes, C. Schwarz, and M. Peitzner, "Aerodynamic investigations of a compressor bleed air configuration typical for aeroengines," in *Proceedings of the XVII International Symposium on Air Breathing Engines (ISABE)*, Munich, Germany, 2005.

[17] C. Schwarz, *Aerodynamische Untersuchungen an Abblase-Luftsystemen mehrstufiger Axialverdichter*, Universität der Bundeswehr München, München (in German), 2005.

[18] V. Peltier, K. Dullenkopf, and H.-J. Bauer, "Experimental investigation of the performance of different bleed air system designs," *Turbo Expo: Power for Land, Sea, and Air*, vol. 44748, pp. 9–21, 2012.

[19] "Pointwise," 2017, http://www.pointwise.com/.

[20] A. Bohne and R. Niehuis, "Experimental off-design investigation of unsteady secondary flowphenomena in a three-stage axial compressor at 100% nominal speed," in *Unsteady Aerodynamics*, K. C. Hall, R. E. Kielb, and J. P. Thomas, Eds., pp. 369–380, Aeroacoustics and Aeroelasticity of Turbomachines, Springer, Dordrecht, 2006.

[21] H. Zimmermann, "Some aerodynamic aspects of engine secondary air systems," *Journal of Engineering for Gas Turbines and Power*, vol. 112, no. 2, pp. 223–228, 1990.

[22] E. M. Greitzer, C. S. Tan, and M. B. Graf, *Internal Flow: Concepts and Applications*, Cambridge University Press, Cambridge, UK, 2007.

[23] G. J. Williams, "Internal flow systems," *International Journal of Heat and Mass Transfer*, vol. 23, no. 4, pp. 577–577, 1980.

[24] I. E. Idelchik, *Handbook of Hydraulic Resistance*, Hemisphere Publishing Corp, Washington, 1986.